PII: S0032-3861(97)00145-6

Polymer Vol. 38 No. 23, pp. 5735–5747, 1997

0032-3861/97/$17.00 + 0.00

Comparison of lamellar thickness and its distribution determined from d.s.c., SAXS, TEM and AFM for high-density polyethylene films having a stacked lamellar morphology

Hongyi Zhou and G. L. Wilkes*
Chemical Engineering Department, Virginia Polytechnic Institute and State University, Blacksburg, VA 24061, USA
(Received 6 September 1996; revised 27 January 1997)

Lamellar thickness and its distribution in high-density polyethylene (HDPE) films having a well-defined stacked lamellar morphology were investigated by using differential scanning calorimetry (d.s.c.), small-angle X-ray scattering (SAXS), transmission electron microscopy (TEM) and atomic force microscopy (AFM). It was found that the most probable lamellar thicknesses from SAXS and TEM agrees very well; however, they do not agree with those values obtained from d.s.c. and AFM. It is pointed out that the use of d.s.c. as a tool to determine lamellar thickness and its distribution is so sensitive to the rate of heating in the d.s.c. experiments and the parameters in the Gibbs–Thomson equation that it is not believed to be suitable for routine quantitative analysis. © 1997 Elsevier Science Ltd.

(Keywords: HDPE; lamellar thickness; lamellar distribution)

INTRODUCTION

Semicrystalline polymers often show a broad melting peak by d.s.c., and this is usually attributed to the distribution of crystalline lamellae thickness[1], although certainly the potential for defect concentration to affect melting is also recognized. Lamellar thickness distribution for a specific polymer is the result of its chemistry and crystallization kinetics, and it also helps account for the thermal and mechanical properties possessed by that specific material. Therefore, it is of interest and desirable to be able to determine this distribution.

D.s.c. melting endotherms can, in principle, be used to calculate the lamellar thickness distribution. In this approach, a d.s.c. profile, heat flow *versus* temperature, is transformed into a lamellar thickness distribution curve (probability of the weight percentage of lamellae *versus* lamellar thickness) by using the Gibbs–Thomson equation[2]

$$T_m = T_m^0\left(1 - \frac{2\sigma_e}{\Delta H_f L}\right) \tag{1}$$

where T_m is the observed melting temperature for a crystalline lamella of thickness L; T_m^0 is the equilibrium melting temperature of the crystalline lamella of infinite thickness; σ_e is the surface energy of the basal surface of the crystalline lamella, and it is associated with the energy of chain folding during the crystallization process; and ΔH_f is the enthalpy of fusion for the crystalline phase. It needs to be pointed out that the above equation is valid only for lamellae whose lateral dimensions are much larger than their thickness, which is generally the case. In certain instances, the precise version of the Gibbs–Thomson equation, which takes into account the surface energy of the side surface and lateral dimensions of the crystalline lamella, would have to be utilized[3].

Because of its simplicity and rapidity, the d.s.c. approach has been used as the principal route by several authors to obtain lamellar thickness and its distribution[4–9]. However, there have been some uncertainties about this approach. There are two different ways to calculate the probability of the lamellar thickness distribution curves. The first method is to use d.s.c. endotherms directly; specifically, the melting endotherms are assumed to be proportional to the weight fraction of crystalline lamellae that melt at a specific temperature (thickness). The second method is to use a differential equation, developed by Alberola *et al.*, based on the mathematical equality of mass fraction of crystalline phase to the ratio of the normalized heat of melting to the enthalpy of fusion, which has led to the following formula[5]:

$$\frac{1}{M}\frac{dM}{dL} = \frac{dE}{dT}\frac{(T_m^0 - T_m)^2}{2\sigma_e T_m} \tag{2}$$

where M is the mass of crystalline phase within the sample for the d.s.c. experiment; dM is the mass of the crystalline phase that melts between T and $T + dT$ with a thickness in the range L and $L + dL$; and dE/dT, obtained from a d.s.c. endotherm, is the energy required to melt the dM fraction of the crystalline phase. All the other parameters in the above equation have the same definitions as in equation (1).

While the above approach seems reasonable at first sight, for accuracy, the effects of heating rate used in the

* To whom correspondence should be addressed

d.s.c. experiments on the obtained lamellar thickness distribution curves must be properly addressed. For example, it is well known that the different heating rate can change the amount of heat flow and shift the temperature reading in the d.s.c. profile. In addition, this same variable can alter the width of a melting peak dramatically[10,11]. These latter factors have not been investigated in the past references given above, and this puts the calculated distribution curves into question. Furthermore, the possibility of annealing effects (e.g. lamellar thickening, partial melting, premelting and recrystallization) for polymer samples during the d.s.c. experiments is also of concern.

There are other approaches that have also been utilized in the literature to determine the lamellar thickness distribution, and they include experimental techniques such as gel permeation chromatography (g.p.c.)[12,13], small-angle X-ray scattering (SAXS)[14,15], transmission electron microscopy (TEM)[16–21], and Raman longitudinal acoustic mode (LAM)[22,23]. The g.p.c. method is based on the fact that nitric acid oxidizes the amorphous phase at a much faster rate than the crystalline phase[11]. As a first attempt to obtain lamellar thickness distribution, the molecular weight distribution measured by g.p.c. experiments for a sample whose amorphous phase is fully removed by the oxidation process was used as an indication of lamellar thickness distribution, which remains intact during the oxidation process[12]. Clearly, this approach is not necessarily a good one due to the complex crystallization process experienced and morphologies possessed by the samples, let alone the difficulties with uniformity of oxidation promoted by limitation on diffusivity and accessibility by the oxidation agent, etc.

SAXS is also a well-established method for the structural investigation of semicrystalline polymers[14,15]. In a simple case, SAXS profiles for semicrystalline polymers having a lamellar morphology in an unoriented state, after proper correction (e.g. Lorentz correction), are generally characterized by one or more diffuse maxima, and the first maximum at the lowest scattering angle is frequently converted into the well-known 'long spacing' by applying Bragg's law. If the percentage crystallinity of the sample is known, and assuming that the crystalline lamellae are spaced filling with a single population of thickness, the mass-based most probable lamellar thickness (L_m) can be calculated by using the following relation:

$$L_m = X_c L_c \tag{3}$$

where X_c is the weight per cent crystallinity, generally measured by d.s.c., wide-angle X-ray diffraction or density, and L_c is the long spacing obtained from the SAXS profile by Bragg's law. However, it is non-trivial to extract the lamellar thickness distribution from SAXS data. According to some authors, it can be done only under the assumption that the crystalline lamellae are isotropic stacks of plates with an infinitely extended lateral dimension[14]. Even in this case, the corrected SAXS data have to be smoothed and fitted to some kind of stacked lamellar morphological model with a known lamellar thickness distribution[15]. Therefore, SAXS is not a routine way to obtain the lamellar thickness distribution, although it can provide an estimation of the average lamellar thickness as expressed by equation (3).

In the use of TEM for the determination of the lamellar thickness distribution, most studies of which have been limited to polyethylene, were initiated by the success of the chlorosulfonation treatment for polyolefins, especially high-density polyethylene (HDPE)[16–20]. Basically, the thickness of crystalline lamellae, as revealed by TEM images taken for samples stained by chlorosulfonic acid and further treated with uranyl acetate, is measured by eye; then the histogram is constructed for the number of measurements *versus* lamellar thickness. From this, a *number*-based lamellar thickness distribution is obtained. The same procedure can also be carried out by using sophisticated image analysis computer programs. The problems associated with the TEM approach are: (1) it is assumed that the morphology of the sample is not altered in the staining process, which is not certain in many cases[21]; (2) the contrast of TEM images is typically not uniform, and this implies that the crystalline lamellae are in different orientation states with respect to the microtomed surface, thus the obtained distribution histograms may not be accurate; (3) the obtained TEM images are only a small fraction of a bulk sample, so it may not be a thorough and accurate representation of the real material. The last problem, however, can be minimized by analysing multiple sections of a given material.

The positions, intensities and shapes of the low-frequency Raman-active band (wavenumber less than 60 cm^{-1}) have been extensively used in the determination of the extended chain length in semicrystalline polymers, again particularly for HDPE[22,23]. It has been shown that the observed integrated intensity is proportional to the length of the ordered sequence, i.e. extended chain length or 'stem' in the crystalline phase[23]. The silent assumptions in this approach are that the amorphous phase, crystalline lamellar surfaces, and tie chains have no effects on the LAM intensity distribution. Furthermore, corrections have to be made for any chain tilting angle inclination of the chain axis with respect to the basal surface of crystalline lamellae.

When practically possible, a combined approach is desirable to make sure that the lamellar thickness distributions obtained from the different approaches have a reasonable agreement. Studies have been published where the lamellar thickness distributions obtained by TEM, SAXS and LAM were compared for linear polyethylene samples (from low and intermediate to high molecular weight) with five different lamellar morphologies[18,19]. Except for samples with fairly narrowly distributed stacked lamellae, where good agreement between the three methods was achieved, limited agreement was found for samples with curved lamellar morphologies or samples with asymmetric or broad lamellar thickness distributions.

Also, there have been studies in which d.s.c., SAXS and TEM were used to obtain lamellar thickness and its distribution[6,7]. In these cases, the most probable lamellar thickness obtained from TEM and/or SAXS was used to 'fit' the lamellar thickness distribution curves generated from the d.s.c. data. From this the surface energy of the basal surface was estimated by using equation (2). Obviously, the equality of the most probable lamellar thicknesses obtained from these approaches needs to be proven.

The purpose of this paper is to present an investigation of lamellar thickness and its distribution by using d.s.c.,

SAXS, TEM and atomic force microscopy (AFM) techniques and to compare the results thus obtained. The materials used in this study were HDPE films having a well-defined stacked lamellar morphology prepared by melt extrusion. The presence of thin lamellar morphology with large lateral dimension ensured the applicability of the Gibbs–Thomson equation. The d.s.c. curves for this material, obtained at a heating rate of $10°C\,min^{-1}$, showed a relatively sharp melting peak, indicating a 'narrow lamellar thickness distribution'. The TEM images for samples treated by chlorosulfonic acid revealed a uniformly good contrast of crystalline lamellae compared with that of the amorphous phase, and thus this simplified stacked lamellar morphology allowed us to develop a confident construction of the lamellar thickness distribution histograms.

With the rapid advances in the application of AFM in polymers, crystalline lamellae have been observed by many authors for different kinds of semicrystalline polymers[23–25]. However, AFM is a surface-oriented tool, and the authenticity of the obtained images has been questioned, especially for experiments done in contact modes[26]. With the development of more advanced skills such as the Tapping Mode or Lift Mode, the application of this technique will certainly become more and more common. The crystalline lamellae in the melt-extruded HDPE films used in this study were 'edge-on' with respect to the film surfaces, and this allowed the direct visualization of the lamellae on untreated film surfaces. Therefore, it is of interest to see whether or not the lamellar thickness distributions for our materials with simple and well-defined stacked lamellar morphologies obtained from AFM are in agreement with the results obtained by the other techniques.

EXPERIMENTAL

Materials

The film materials used in this study were prepared from an HDPE resin with a number-average molecular weight (M_n) and weight-average molecular weight (M_w) of 14 500 and 150 000 $g\,mol^{-1}$, respectively. The films (1 mil (0.0254 mm) in thickness) were extruded under processing conditions such that the crystalline phase is quite highly oriented along the machine direction, whereas the amorphous phase is essentially in a random state. A detailed study of the orientation state of crystalline phase and amorphous phase of the films used in this study has been provided elsewhere[27]. In addition to the extruded film, which was designated as precursor film (Pre), two annealed films of this same precursor were also utilized. The annealed films were prepared by annealing at 120 and 130°C for 20 min; based on earlier experiments, 20 min of annealing at these temperatures is sufficient for the majority of lamellae thickening. The two annealed materials were designated as F120 and F130, respectively.

D.s.c. experiments

A Perkin Elmer DSC-7 instrument was used for all the d.s.c. experiments. D.s.c. scans were carried out by using seven different heating rates of 1, 2, 4, 8, 16, 32 and 64°C min^{-1}. Baseline calibrations were made for all the heating rates. A small, fixed sample weight (~3.0 mg) was used, and all the d.s.c. samples had the same shape and size—four layers of circular 1 mil (0.0254 mm) films with the same diameter as the d.s.c. sample pan. All the samples were sealed in the same manner by using a pan crimping tool in order to ensure good sample–pan contact. For comparison, a standard indium (In) sample was also scanned at the seven heating rates used for the HDPE samples. When applying the Gibbs–Thomson equation to the d.s.c. data, the ΔH_f, σ_e and T_m^0 values utilized were 290 $J\,cm^{-3}$, 90 $mJ\,m^{-2}$ and 145.5°C, respectively[28].

SAXS experiments

A standard Kratky slit-collimated camera was used for the SAXS experiments. Stacks of HDPE films were used as the samples for the SAXS experiments. In order to minimize the effect of orientation, nine layers of films were used in each stack, and the machine direction (MD) of each layer of film within the stack was at an angle (~11°) with respect to the adjacent layer of film so that the MDs were uniformly distributed in the plane of the sample holder. The same sample stacks were also studied by a separate synchrotron X-ray scattering experiment, and the results showed several isolated first-order scattering 'spots' at the same scattering angle—each pair of which arises from a film layer with a specific orientation. Thus, the azimuthal intensity distribution is not perfectly circularly uniform, which should be the case for a truly isotropic media. However, more importantly for this study, the long spacing for the specific sample obtained from the synchrotron experiment was found to be in good agreement with that from the Kratky experiment on the same sample.

TEM experiments

Samples for the TEM study were stained with chlorosulfonic acid at 60°C for 6 h, then washed with sulfuric acid and water. After being dried overnight, the samples were embedded in an epoxy resin and cured overnight at 65°C. The embedded samples were microtomed at room temperature, and the microtomed thin sections were ~80 nm thick. All the TEM experiments were performed using a Philips EM420 instrument operated at 100 kV.

AFM experiments

Samples for the AFM experiments were the untreated film surfaces. Double sided tape was used to mount the sample to the sample stage. All the AFM experiments were carried out using a NanoScope III SPM (Digital Instrument) instrument operating in the Tapping Mode. In this mode, a silicon tip oscillating slightly below its resonance frequency (~200 kHz) hovers above the surface of the sample at a very short distance (50–150 Å). The tip–sample interaction was short and intermittent to prevent surface deformation during the experiments. The output images were collected in the form of height image amplitude images. The lamellar thickness estimates were done by using the amplitude image mode.

RESULTS

Figures 1a–1c are the d.s.c. scans at the seven heating rates for the three HDPE films used in this study. The effects of heating rate are clearly shown. Once the heating rate was doubled, the melting endotherm (the area under the melting peak) was also doubled (the sample weight

was kept constant), and this can be justified by the fact that the heat flow (dE/dt) measured by the d.s.c. instrument is dependent on time (dt), or heat rate (dT/dt), used in the experiment. There was also a shift to higher temperatures for the melting endotherms as the heating rate was increased. More prominently, the width of the melting peaks was dramatically changed by the heating rate. The same effects also existed for the standard In sample, which can be noted in *Figure 1d*. Since the In sample has a better thermal conductivity, the thermal lag was less pronounced than that for the HDPE samples. Nevertheless, the intrinsic thermal lag in the d.s.c. experiments always exists.

Therefore, in order to use the d.s.c. data for the

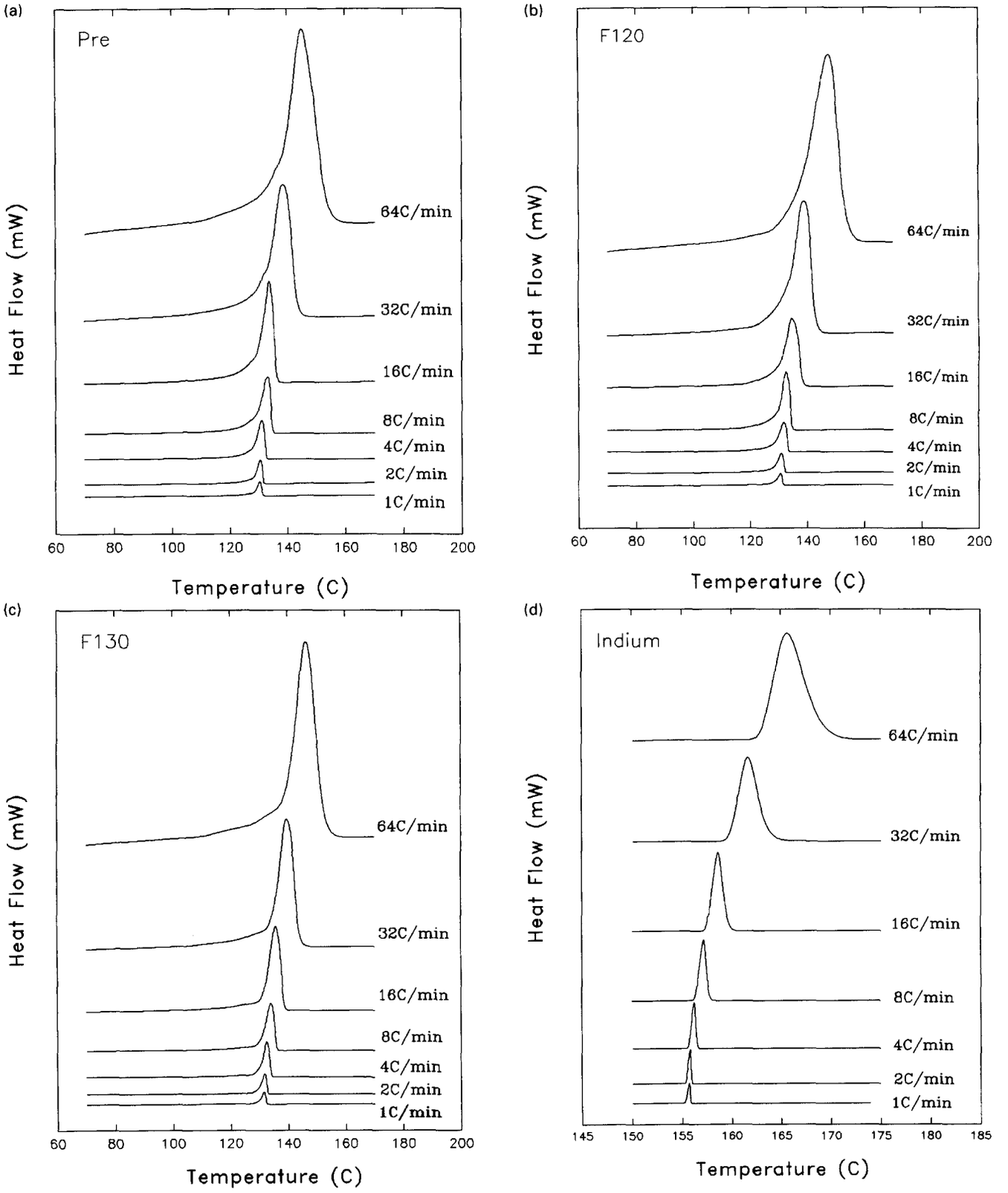

Figure 1 D.s.c. scans at seven different heating rates for (a) precursor film, (b) annealed film at 120°C, (c) annealed film at 130°C and (d) standard In sample

calculation of the lamellar thickness distribution, corrections for thermal lag have to be made. To do this, the heat flow was normalized by the heating rate, converting dE/dt into dE/dT. Secondly, the d.s.c. curves were shifted to 'zero heating rate'; this was done by constructing a plot of melting temperature (peak temperature in the d.s.c. melting endotherm) *versus* heating rate, as shown in *Figure 2*. It was noted that in *Figure 2* at slow heating rates the peak melting temperatures for the precursor film and the F120 film were almost identical, and this is an indication that the precursor film was probably 'annealed' during the d.s.c. scan at the slowest heating rate. Therefore, the extrapolations were done without using the d.s.c. data for the 1 and 2°C min^{-1} heating rates. No attempts were made to make any correction for the width of the melting peaks since the relationship between the width of a d.s.c. melting peak and heating rate is non-linear[9]. In addition, due to the above-mentioned annealing effect during the d.s.c. experiment, it is not possible to know the exact width of the melting peaks for the initial (original) lamellar morphology at the lower heating rates. Using this approach, the corrected d.s.c. data for the three HDPE films are shown in *Figure 3*.

Figures 4 and *5* show the calculated lamellar thickness distribution from the corrected d.s.c. data. The two methods described in the introduction to this paper were then both applied to the data, i.e. the 'direct' approach of the Gibbs–Thomson equation and the 'indirect' approach which uses differential equation (2). *Figure 4* provides the results obtained from the method in which the d.s.c. melting endotherms were used directly, while *Figure 5* displays the results of the method in which the differential treatment (equation (2)) was used. The most probable lamellar thickness, the value that corresponds to the peak position in the distribution curve, is shown on each distribution curve. It can be seen in *Figure 4* that the most probable lamellar thickness was the same because of the shifting to 'zero-heating rate' of the d.s.c. data. In *Figure 5*, however, this is not the case—the most probable lamellar thickness decreased at higher heating rates. *Figures 4* and *5* show that the distribution curves are different at different heating rates, and the two ways to calculate the probability result in different distribution curves at the same heating rate, although they are quite similar at slower heating rates.

The SAXS data are shown in *Figure 6*, where intensities before and after the Lorentz correction are plotted against the scattering vector (defined as $S = (2/\lambda)\sin\theta$, where θ is one-half of the scattering angle). Since the special film stacks were used as samples for SAXS experiments, the Lorentz correction factor used was the same as that for the standard slit-collimated SAXS data. Annealing not only 'sharpened' the scattering peaks, but also moved them to lower scattering angles, indicating an increase in the long spacing. In addition, a well-defined second-order scattering peak was also present for the annealed films. The most probable lamellar thickness, L_m, calculated by using equation (3), is also shown in this figure. In the

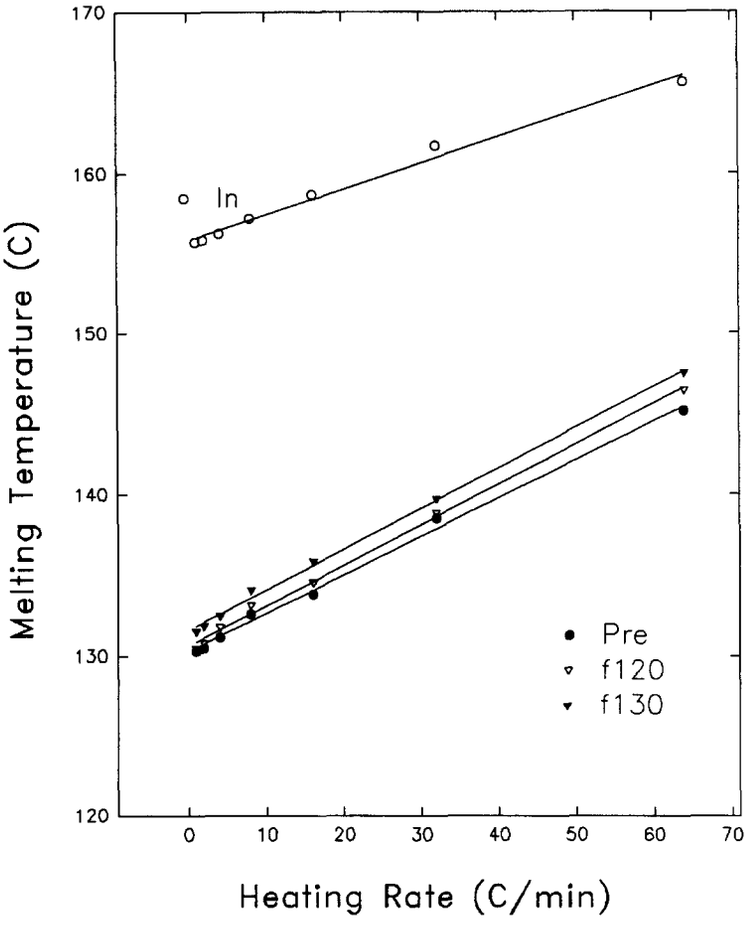

Figure 2 Linear relationship between melting temperature (melting endotherm maxima) and heating rate for precursor film, annealed films at 120 and 130°C and In

calculations, the percentage crystallinities used were from the d.s.c. experiments, being 61, 71 and 78% for pre, F120 and F130 films, respectively. No attempt was made to calculate the lamellar thickness distribution from the SAXS data.

The TEM results are presented in *Figure 7*, where electron micrographs for the two annealed HDPE films are shown. Lamellar thickness distribution histograms based on the TEM images were constructed and are shown in *Figure 8*. Only the results for the two annealed films are presented, since the TEM images for the precursor film did not provide a sufficiently sharp contrst to allow a confident measurement of lamellar thickness. Over 300 lamellae in five different micrographs taken under the same conditions were used for these distribution histograms. Only those lamellae that displayed

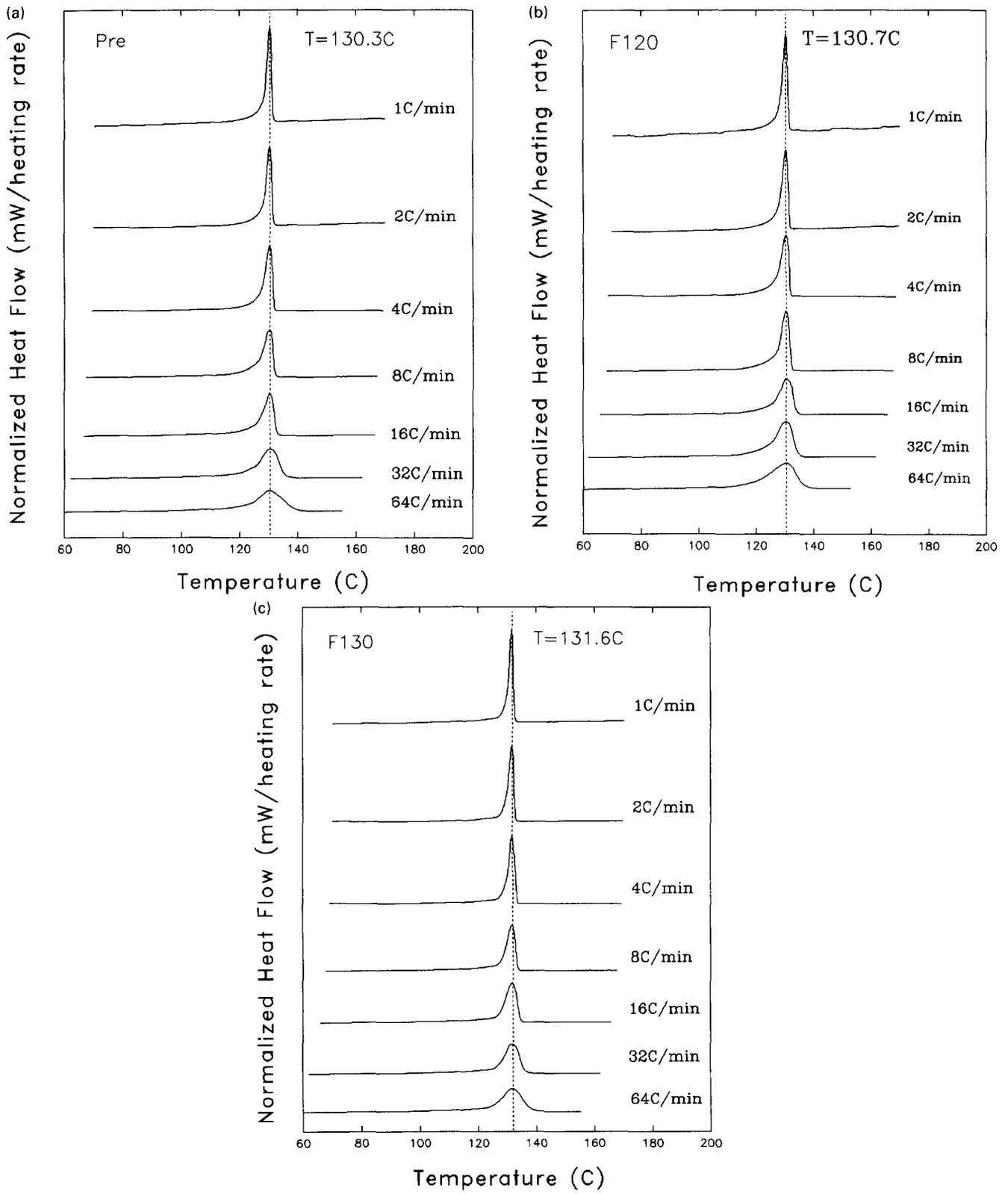

Figure 3 Normalized and shifted d.s.c. data for (a) precursor film, (b) annealed film at 120°C and (c) annealed film at 130°C

uniform and sharp contrast and had straight and large lateral dimensions were selected, and by doing this the effect due to the different orientations of the crystalline lamellae with respect to the microtoming were believed to be minimized.

In order to compare the results with those from d.s.c., the number-based distribution histograms have to be transformed into mass-based distribution histograms. The mass-based distribution histograms were obtained by multiplying the 'probability' of the number-based distribution histograms by the corresponding lamellar thickness—in doing this we are using the assumption that all the counted lamellae had the same lateral surface area, which may not be fully justified but is a reasonable first approximation for the type of stacked lamella system we are investigating here.

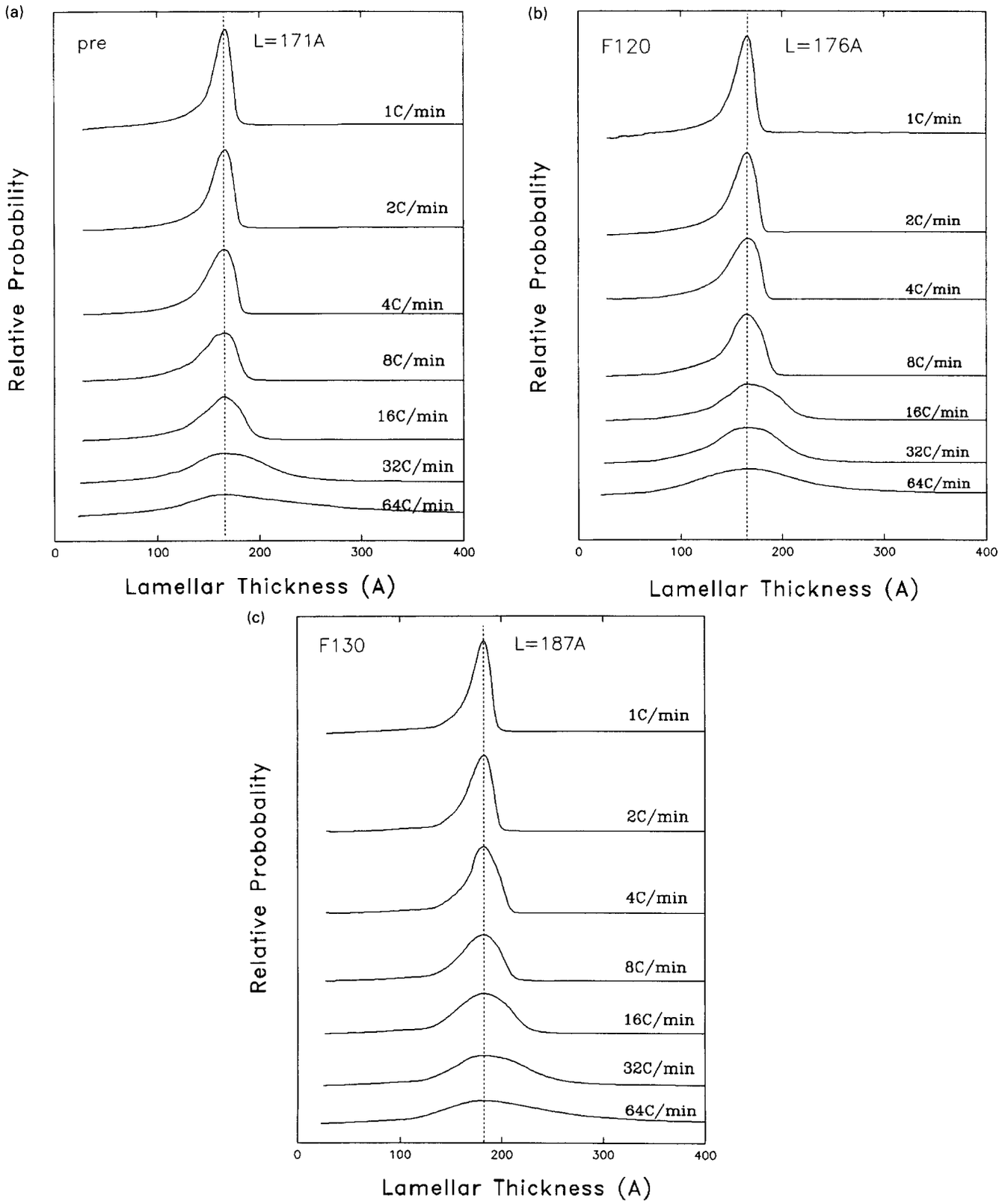

Figure 4 Lamellar thickness distribution curves for (a) precursor film, (b) annealed film at 120°C and (c) annealed film at 130°C calculated by directly using the corrected d.s.c. data (melting endotherms)

Figure 9 presents the Tapping Mode AFM images (amplitude images) obtained for the annealed films. Only images for the two annealed films are shown since the image for the precursor film was not satisfactory for lamellar thickness measurement. The histograms generated from AFM are presented in *Figure 10*. The measurement of the lamellar thickness was done by directly using the analysis software of the AFM instrument. The same lamellae selection criteria was used as in the TEM experiment. The mass-based distribution histograms were also constructed by using the same method as in the TEM experiments. The number of lamellae used in the construction of the histograms in this case was over 200 from five AFM

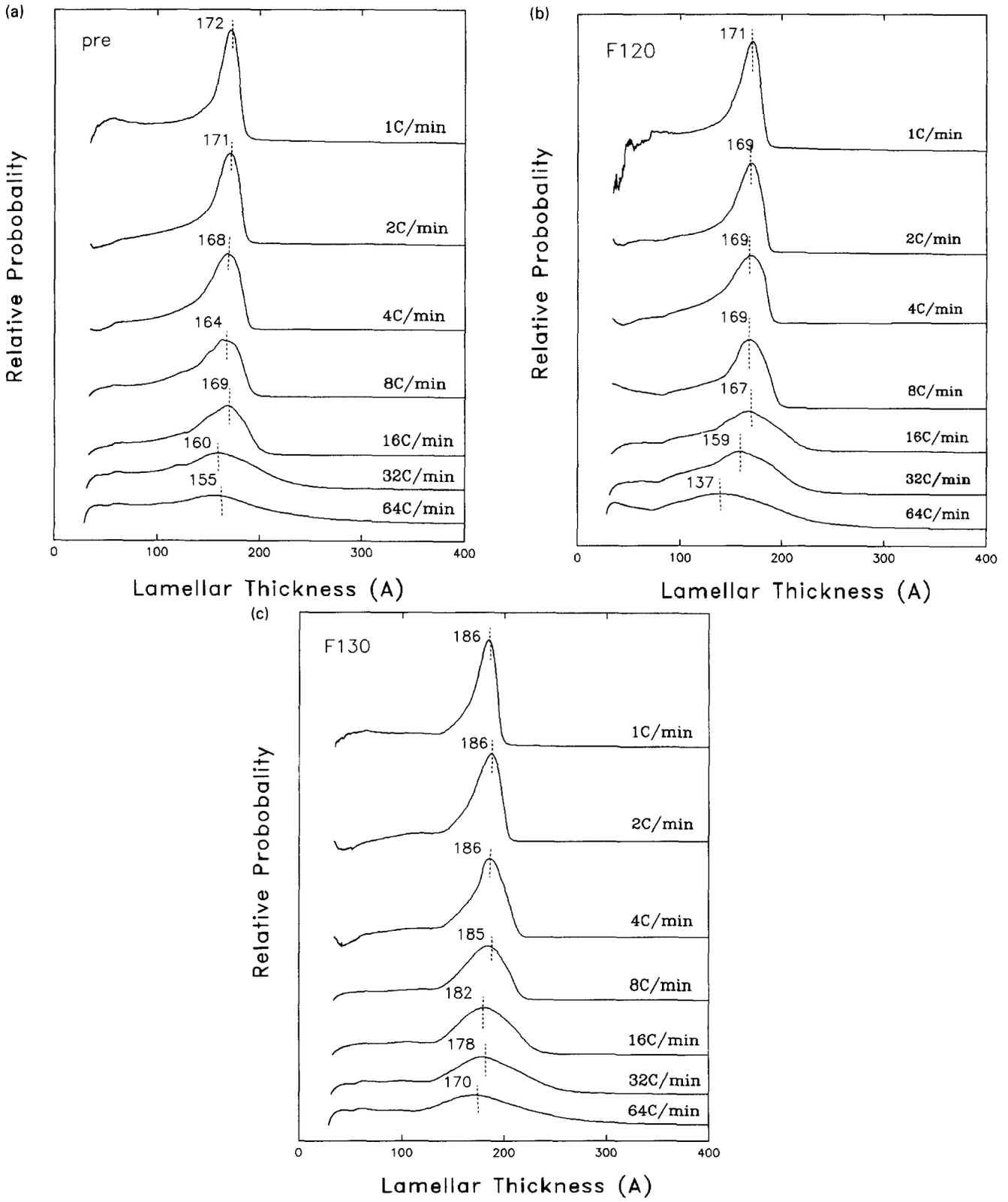

Figure 5 Lamellar thickness distribution curves for (a) precursor film, (b) annealed film at 120°C and (c) annealed film at 130°C calculated by using the differential equation (2)

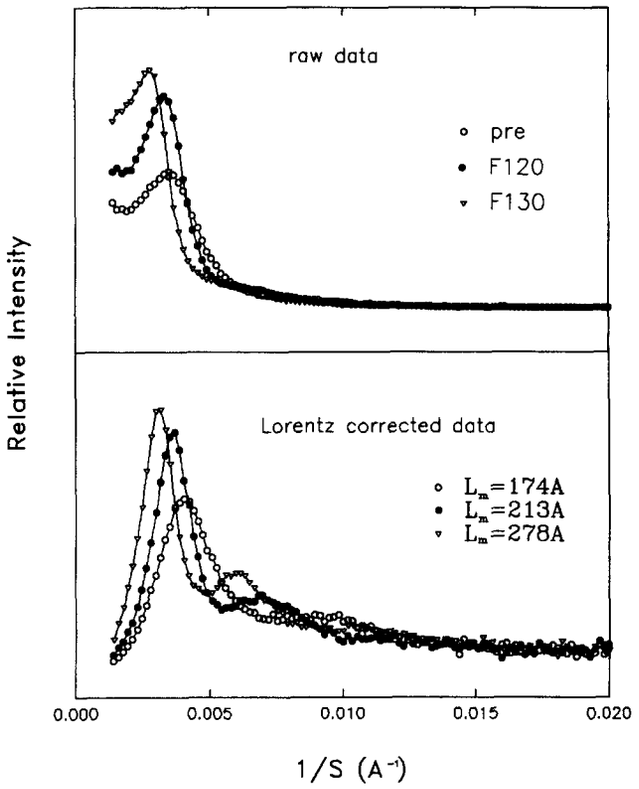

Figure 6 SAXS profiles (before and after Lorentz correction) for precursor film (Pre), annealed film at 120°C (F120), and annealed film at 130°C (F130)

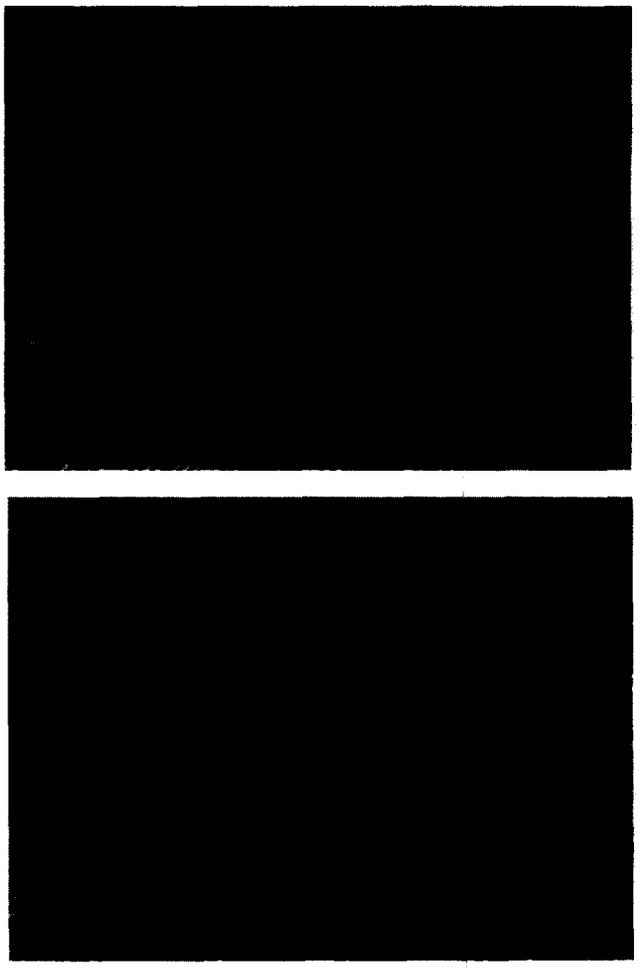

Figure 7 TEM images for annealed films at (a) 120°C and (b) 130°C. The scale bars represent 300 nm

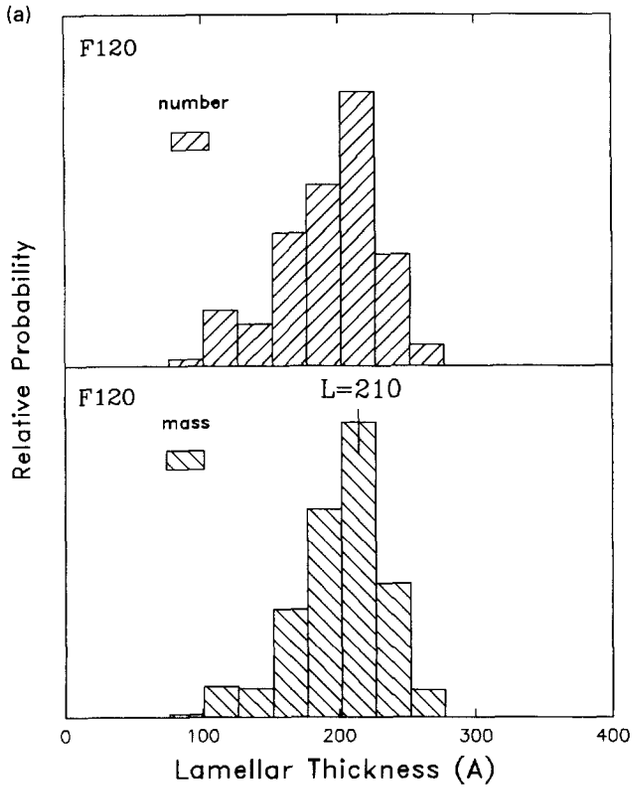

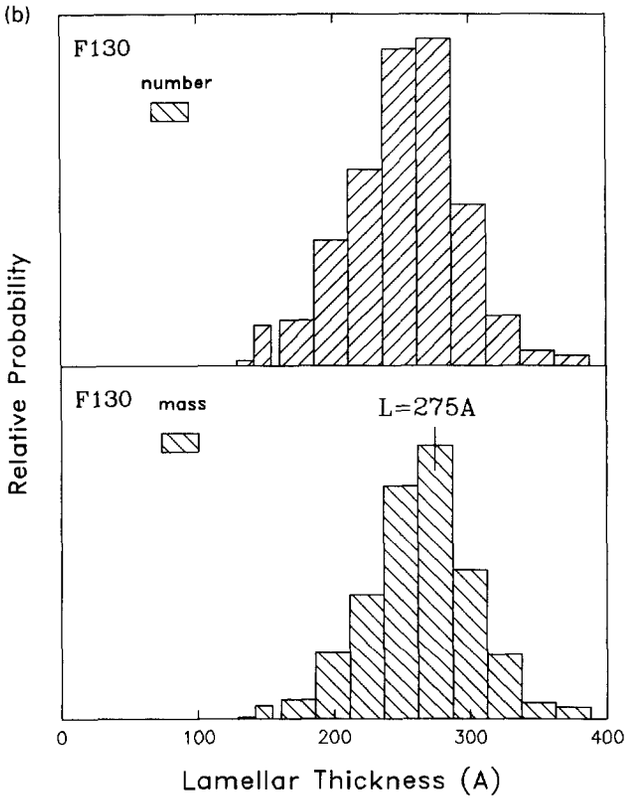

Figure 8 Lamellar thickness distribution histograms based on TEM results for annealed film at (a) 120°C and (b) 130°C

images for each histogram. It was noticed that the data were scattered and the maxima were less well defined as compared with the TEM results, and this is probably due to the untreated sample surfaces used in the experiments.

DISCUSSION

Most probable lamellar thickness

Comparing the most probable lamellar thickness obtained from SAXS, TEM and AFM, it was found that for the F120 and F130 films, the values from SAXS and TEM were in surprisingly good agreement, with the average lamellar thickness being 213 and 278 Å from SAXS and 210 and 275 Å from TEM. The same conclusion has been drawn by others for HDPE samples[18,19]. The values from AFM seem to be larger than those from SAXS and TEM, being 240 and 310 Å, respectively, for F120 and F130 films. However, because of the lack of a well-defined maxima in the distribution curves based on the AFM experiments, these average values carry somewhat less meaning.

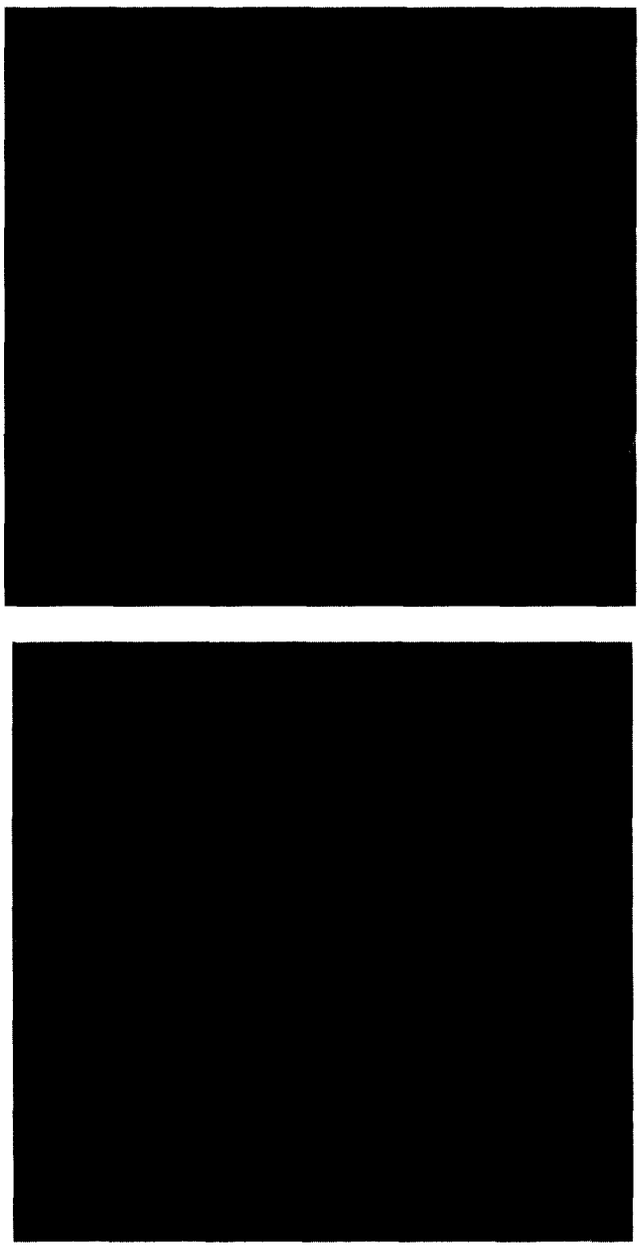

Figure 9 AFM images (amplitude images) for annealed films at (a) 120°C and (b) 130°C. The scale bars represent 400 nm

Regarding the AFM results, it must be clearly recognized that the lamellar morphology on a film surface may not be the same as in the bulk. For solution-grown, ultra-thin and ultra-drawn HDPE films, the crystalline phase was found to protrude out of the film surface as observed by AFM[23], and the same phenomenon was also observed for melt-extruded films[29,30]. This has been explained by the authors as a combination of film processing and crystal growth. We recognized that our materials do not have the same kind of morphology as the above-described ultra-thin films; however, we indeed found a larger most probable lamellar thickness (although not well defined and with a wide range) on the surface of our films compared to the TEM results, which were based on bulk samples. One possible reason for this difference, which seems to be more pertinent for the melt-extruded films used in this study, is the likelihood of 'fold-over' of the crystalline lamellae. Fold-over may be introduced due to the friction between the film surface and other surfaces (e.g. film-collecting spool) during or after the process of crystallization; and because of this, the crystalline lamellae on the surface seems to be thicker, as observed by the AFM experiment.

On the other hand, AFM is basically a surface characterization technique. In fact, the contrast of AFM images is based on surface roughness in the cases of height and amplitude imaging. The surface roughness of our samples (the melt-extruded film and annealed films) can be influenced by many factors, from microscopic molecular relaxation to macroscopic die smoothness. Therefore, in order to make a fair comparison for the lamellar thickness and its distribution, measurements on samples cryomicrotomed from bulk materials would be more desirable. That is, ideally, one would like to use a virgin HDPE sample without staining, cryomicrotome it, collect the microtomed thin sections for TEM observation, and use the surface on the bulk part of the sample for AFM observation. Since the films were uniaxially oriented, the microtoming can be done by simply cutting in the plane that contains the MD and ND (normal direction) of the films. Unfortunately, although we have tried to do this, we have not been able to successfully make such measurements.

The most probable lamellar thickness from d.s.c. data, provided either in *Figure 4* or *5*, was influenced by the heating rate of the d.s.c. experiment. By shifting to 'zero heating rate', the melting temperature for samples Pre, F120 and F130 were 130.3, 130.7 and 131.6°C, respectively; these temperatures, according to equation (2), correspond to lamellar thicknesses of 171, 176 and 187 Å. These values were less than those from SAXS and TEM (174, 213 and 278 Å for the respective three films), with the exception for the Pre film, which is not easily explained. If the most probable lamellar thickness from SAXS was used in equation (2), the calculated melting temperatures for the Pre, F120 and F130 films would be 130.2, 133.2 and 135.8°C, respectively. Based on *Figure 2*, these melting temperatures would then correspond to heating rates of 0, 10 and 17°C min^{-1} in the d.s.c. experiments for the three films. Therefore, except for the Pre film, shifting the d.s.c. data to 'zero heating rate' did not give rise to a most probable lamellar thickness result that agrees with the other techniques.

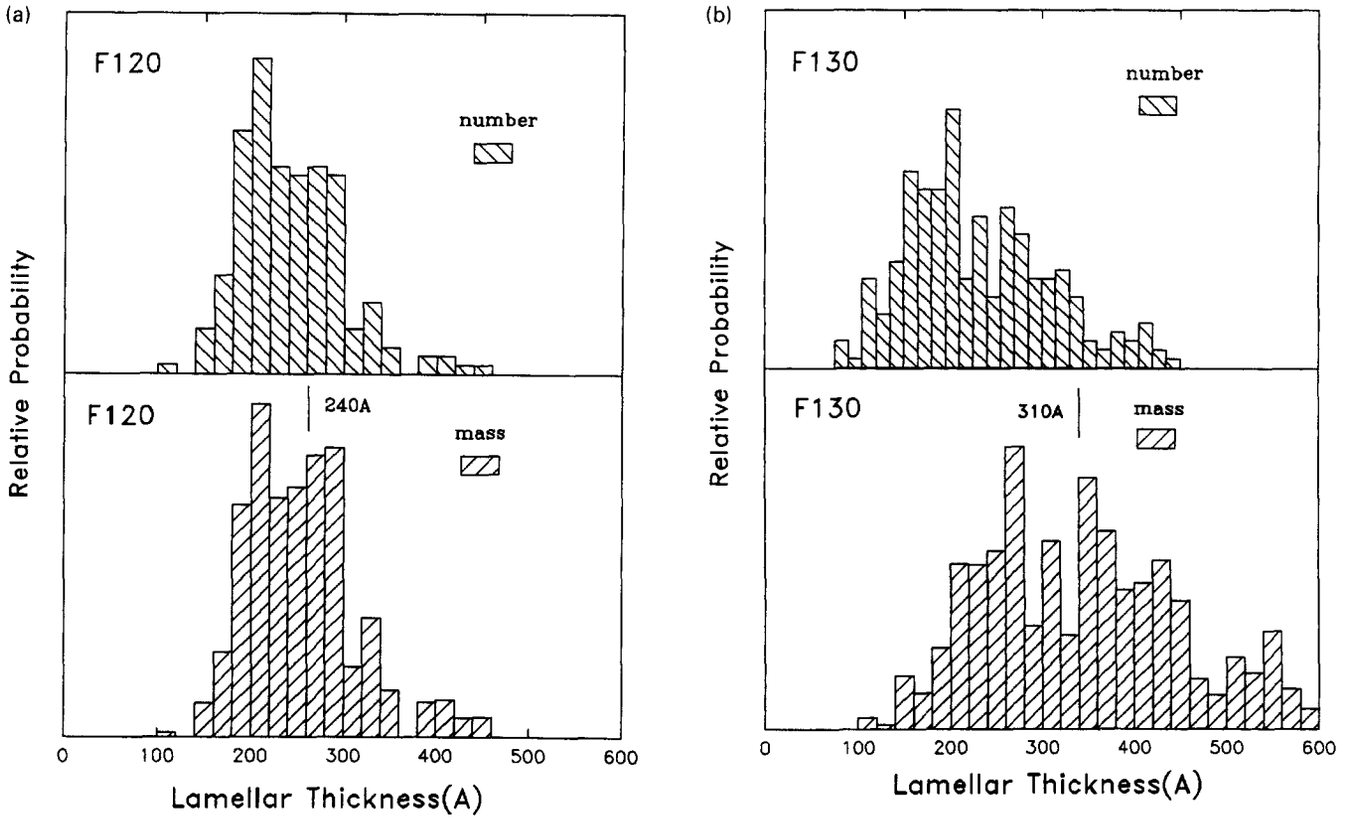

Figure 10 Lamellar thickness distribution histograms based on TEM results for annealed film at (a) 120°C and (b) 130°C

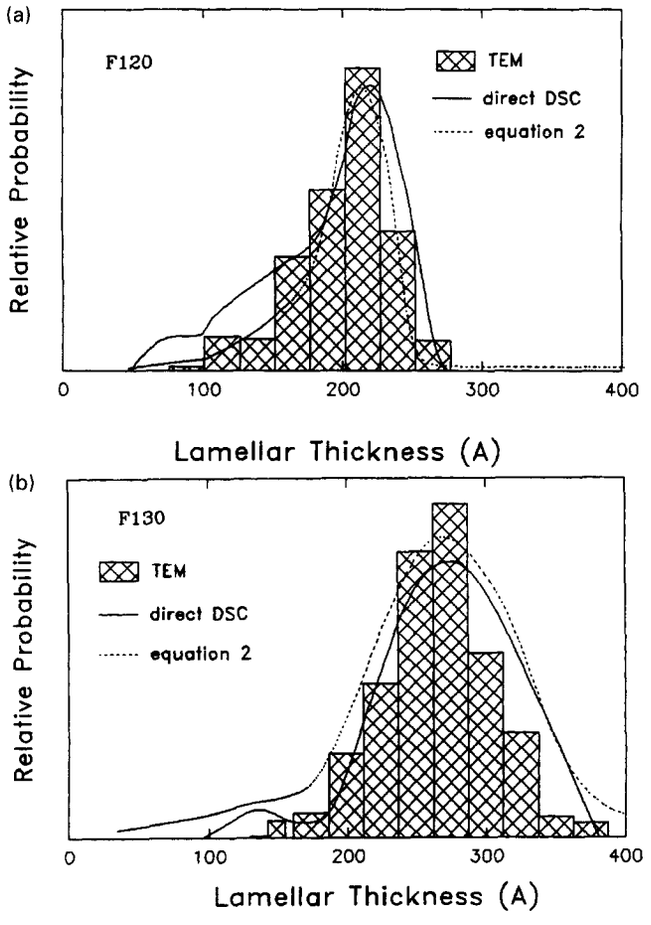

Figure 11 Overlay of lamellar thickness distribution curves, from *Figure 4* at 8°C min^{-1} heating rate (dotted lines) and from *Figure 5* at 16°C min^{-1} heating rate (solid line), and distribution histograms from *Figure 8*. The results shown here are for annealed films at (a) 120°C and at (b) 130°C

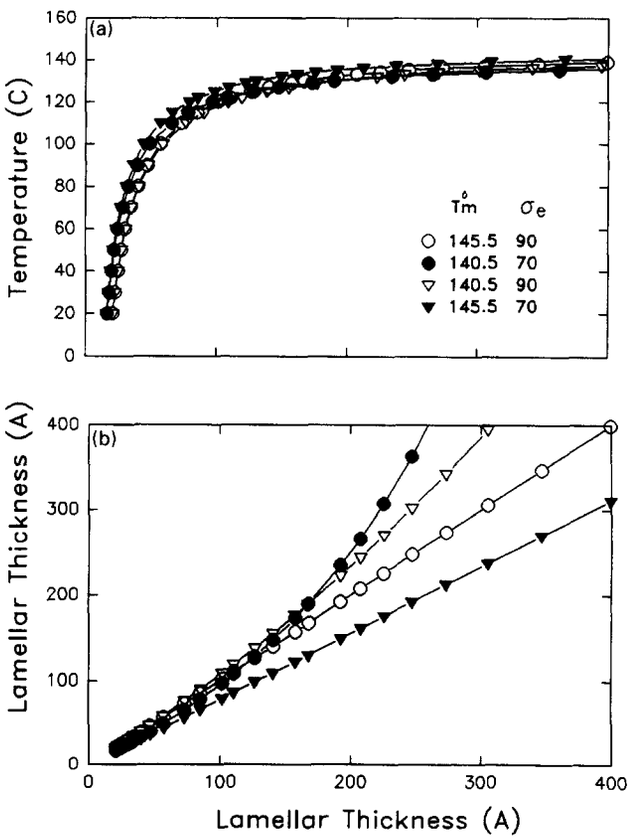

Figure 12 Effects of equilibrium melting temperature (T_m^0) and surface energy (σ_e) on the calculated lamellar thickness using the Gibbs–Thomson equation

Lamellar thickness distribution

The lamellar thickness distribution curves calculated from d.s.c. data (*Figures 4* and *5*) clearly show large differences caused by heating rate, i.e. from very narrow distributions at lower heating rates to very broad distributions at higher heating rates. This observation holds true no matter which of the two methods was used to calculate the probability of the distribution curve. At smaller heating rates, thermal lag was minimized, but the materials were subject to annealing during the d.s.c. experiment; thus the determined distribution curves did not truly represent the original samples. At higher heating rates, the original morphology was undoubtedly better preserved; however, the effect of thermal lag is undoubtedly more pronounced, thus the distribution curves are likely to be partially in error. Therefore, the distribution curves are highly heating rate sensitive, as shown earlier in *Figures 4* and *5*.

In most of the published work where d.s.c. has been used as a tool to obtain the lamellar thickness distribution, the quoted lamellar thickness distributions have been based on experiments carried out at a single heating rate, commonly 10°C min^{-1}. We also plotted the lamellar distribution curves calculated by using the original (unshifted) d.s.c. data at heating rates of 8 and 16°C min^{-1} for the F120 and F130 films, and the results are presented in *Figure 11*. Dotted lines and solid lines correspond to the two ways of calculating the probability which were used to construct *Figures 4* and *5*. Also included in *Figure 11* are the lamellar thickness distribution histograms obtained by TEM for the same annealed films. We were surprised to find that there was reasonable agreement for not only the most probable lamellar thickness but even for the entire distribution!

It was pointed out earlier that the width of a d.s.c. melting peak is affected by heating rate in a non-linear fashion, and hence so is the lamellar thickness distribution based on the d.s.c. data. Thus, an appropriate heating rate should help balance the thermal lag effect, which tends to broaden the melting peak (distribution curve), and the annealing effect, which tends to narrow the melting peak (distribution curve). Examining the lamellar thickness distribution curves again in *Figures 4* and *5*, it was noted that these curves were similar in the heating rate range between 8 and 16°C min^{-1}. While no proof exists, these two heating rates may be in the appropriate range for the d.s.c. experiment that generates the more nearly accurate lamellar thickness distribution curves, as suggested by the TEM method.

Additional support for this 'coincidence' extends perhaps from the excellent match for the values of most probable lamellar thickness from d.s.c. and those from TEM and/or SAXS, as shown in *Figure 11*. The heating rates calculated by equation (2) based on the lamellar thickness from SAXS and/or TEM were 10 and 17°C min^{-1} for F120 and F130, respectively, and these heating rates are very close to 8 and 16°C min^{-1} as shown in *Figure 11*, for the same films. Therefore, the apparent agreement between the lamella thickness distributions observed in this study and other investigations seems to be fortuitous rather than expected.

Effects of σ_e *and* T_m^0

Certainly, by using equation (2), the calculated lamellar thickness is affected by the values of the three parameters in equation (2), namely ΔH_f, σ_e, and T_m^0. According to the literature[31–38], 290 J cm^{-3} is a well-accepted value for ΔH_f, which is also what was used in this study. However, the parameter σ_e has values between 70 and 90 mJ m^{-2}, and values quoted for T_m^0 range from 140.5 to 145.5°C. In *Figure 12a* the effects of σ_e and T_m^0 on the calculated lamellar thickness according to equation (2) were presented by using diferent values of σ_e and T_m^0, as shown in this figure. As the temperature increases, a small variation in the equilibrium melting temperature and/or surface energy can result in a large difference in the calculated lamellar thickness. *Figure 12b* shows a comparison between the lamellar thickness calculated in this study by using $\sigma_e = 90$ mJ m^{-2} and $T_m^0 = 145.5$°C (x-axis) and the lamellar thickness (y-axis) if other values of σ_e, and T_m^0 have been used, including the above values. Again, the deviations begin to be prominent starting from ~100 Å, which is the range for the HDPE films used in this study.

Furthermore, the given assumption of using the Gibbs–Thomson equation to calculate lamellar thickness is that the surface energy is a constant. Practically, however, there is the possibility that the surface energy is somewhat changed during the d.s.c. experiments. When the temperature rises during the d.s.c. scans, the mobility of polymer chains increases, especially at temperatures higher than that of the mechanical α relaxation. The basal surface of lamellae can reorganize and therefore decrease the surface energy. The change in surface energy certainly affects the calculated lamellar thickness, as already shown in *Figure 12*. Given the uncertainties about the exact values of σ_e and T_m^0 and the potential change of σ_e, it seems impossible to obtain accurate lamellar thickness values with high confidence by using equation (2).

CONCLUSIONS

Based on the investigations for HDPE films having a well-defined stacked lamellar morphology in this study, it is concluded that the most probable lamellar thickness from SAXS agrees well with that from TEM, but not with those from d.s.c. and AFM. The use of d.s.c. as a tool to determine the lamellar thickness distribution based on the Gibbs–Thomson equation needs be limited for certain heating rates so that the effects of thermal lag and of 'annealing' during the d.s.c. scan are balanced (e.g. 8–16°C min^{-1} for HDPE materials, based on the present study). As for AFM, more work on the experimental technique is necessary before one can finally conclude whether it can be utilized to determine the lamellar thickness distribution. It is worth pointing out that the conclusions given here are based on HDPE films having a well-defined stacked lamellar morphology and relatively narrow melting peaks in the d.s.c. scans at 10°C min^{-1} heating rate. For polyethylene or other materials having more complex morphologies (e.g. spherulitic morphology) and/or having wider melting peaks in the d.s.c. scans (e.g. branched polymers), it is expected that a comparable analysis would be much more difficult—specifically for the direct measurement of lamellar thickness by TEM. Hence, we view our work to be of value as a model study to address the issue of whether the measurement of lamellar thickness and its distribution can be determined with consistency by different standard analytical characterization techniques.

ACKNOWLEDGEMENT

We would like to thank Hoechst Celanese Co. for kindly providing the melt-extruded HDPE films used in this study.

REFERENCES

1. Wunderlich, B., *Macromolecular Physics*, Vol. 3. Academic Press, London, 1980.
2. Hoffman, J. D., *Treatise on Solid State Chemistry*, Vol. 3. Plenum Press, New York, 1976.
3. Rodriguez, J. C., Alonson, M., Merino, M. and Pastor, J. M., *J. Polym. Sci., Phys. Ed.*, 1996, **60**, 1709.
4. Wlochowicz, A. and Eder, M., *Polymer*, 1984, **25**, 1268.
5. Bodor, C., Dalcolmo, H. J. and Schroter, O., *Colloid Polym. Sci.*, 1989, **267**, 480.
6. Alberola, N., Cavaille, J. and Perez, J., *J. Polym. Sci., Polym. Phys. Ed.*, 1989, **28**, 569.
7. Darras, O. and Seguela, R., *Polymer*, 1993, **34**, 2946.
8. Liu, L., Alamo, R. G. and Mandelkern, L., *Macromolecules*, 1994, **27**, 6571.
9. Plummer, C. J. G. and Hausch, H. H., *Polym. Bull.*, 1996, **36**, 355.
10. Wu, Ch., Eder, G. and Janeschitz-Kriegl, H., *Colloid Polym. Sci.*, 1993, **271**, 1116.
11. Janeschitz-Kriegl, H., Wippel, H., Paulik, Ch. and Eder, G., *Colloid Polym. Sci.*, 1993, **271**, 1116.
12. Keller, A. and Udagawa, Y., *J. Polym. Sci. A-2*, 1972, **10**, 221.
13. Mills, P. J. and Hay, J. N., *Polymer*, 1984, **25**, 1227.
14. Crist, B., *J. Polym. Sci., Polym. Phys. Ed.*, 1973, **11**, 635; Crist, B. and Morosoff, N., *J. Polym. Sci., Polym. Phys. Ed.*, 1973, **11**, 1023.
15. Lee, Y. D., Phillips, P. J. and Lin, J. S., *J. Polym. Sci., Polym. Phys. Ed.*, 1991, **29**, 1235.
16. Voigt-Martin, I. G., *J. Polym. Sci., Polym. Phys. Ed.*, 1980, **18**, 1513.
17. Voigt-Martin, I. G. and Fischer, E. W., *J. Polym. Sci., Polym. Phys. Ed.*, 1980, **18**, 2347.
18. Voigt-Martin, I. G. and Mandelkern, L., *J. Polym. Sci., Polym. Phys. Ed.*, 1981, **19**, 1769.
19. Voigt-Martin, I. G. M., Stack, G., Peacock, A. J. and Mandelkern, L., *J. Polym. Sci., Polym. Phys. Ed.*, 1989, **27**, 975.
20. Voigt-Martin, I. G. and Mandelkern, L., *J. Polym. Sci., Polym. Phys. Ed.*, 1989, **27**, 967.
21. Strobl, G. R., *J. Polym. Sci., Polym. Phys. Ed.*, 1981, **21**, 1357.
22. Sander, R. G., *J. Polym. Sci., Polym. Phys. Ed.*, 1980, **18**, 421.
23. Jandt, K. D., Buhk, M., Miles, M. J. and Petermann, J., *Polymer*, 1994, **11**, 2458.
24. Vancso, G.J., Nisman, R., Snetivy, D., Schonherr, H., Smith, P., Ng, C. and Yang, H., *Colloid Surface*, 1994, **87A**, 263.
25. Goldbeck, G., Fischer, H. and Barham, P. J., *Polym. Bull*, 1995, **35**, 183.
26. Quate, C. F., *Surface Sci.*, 1994, **299/300**, 980.
27. Yu, T. and Wilkes, G. L., *Polymer*, 1996, **37**, 4576.
28. Hoffman, J. D., Miller, R. L., Marand, H. and Roitman, D. B., *Macromolecules*, 1992, **25**, 2221.
29. Jandt, K. D., *Untersuchungen zur Polymer-Metall-Epitaxie in Computersimulation und Experiment*, Fortschr, VDI Reihe 5, No. 302, 1993.
30. Eng, L. M., Jandt, K. D., Fuchs, H. and Petermann, J. J., *Helv. Phys. Acta*, 1992, **87**, 870.
31. Hoffman, J. D., Lauritzen Jr, J., Passaglia, I. E., Ross, G. S., Forlen, L. J. and Weeks, J. J., *Kolloid Z. Z. Polym.*, 1969, **231**, 564.
32. Hoffman, J. D., Forlen, L. I., Ross, G. S. and Luritzn Jr, J. I., *J. Res. Natl Bureau Standards*, 1975, **79A**, 671.
33. Kavesh, S. and Schultz, J. M., *J. Polym. Sci. A-2*, 1970, **8**, 243.
34. Wunderlich, B. and Cormier, C. H., *J. Polym. Sci. A*, 1967, **5**, 2987.
35. Arakawa, T. and Wunderlich, B., *J. Polym. Sci. C*, 1967, **16**, 653.
36. Ergoz, E., Fatou, J. G. and Mandelkern, L., *Macromolecules*, 1972, **5**, 147.
37. Broadhurst, M. G., *J. Res. Natl Bureau Standards*, 1966, **70A**, 481.
38. Flory, P. J. and Vrij, A., *J. Am. Chem. Soc.*, 1963, **85**, 3458.